KSME Journal, Vol. 10, No. 3, pp. 341~350, 1996

Aerodynamic Forces of Elliptic-Cone Derived Waveriders at Hypersonic Velocities

Bok-hyun Yoon* and M. L. Rasmussen**

(Received December 17, 1994)

The aerodynamic data for two kinds of elliptic-cone derived waveriders are presented and analyzed for a wide range of Mach numbers and angles of attack. The basic shapes of the waveriders are obtained by means of hypersonic small-disturbance theory. Various off-design performances of the waveriders as well as on-design performances are obtained and fully discussed. These aerodynamic data are informative for the design of hypersonic airplanes which are being investigated as future planes. Also from the entropy distributions across the shock layers for elliptic-cones and waveriders, the vortical layer is analyzed and discussed.

Key Words: Waverider, Hypersonic Flow, CFD, Aerodynamics, Vortical Layer

Nomenclature

A : Axial force
C_A : Axial-force coefficient
C_D : Drag coefficient
C_L : Lift coefficient
C_N : Normal-force coefficient
D : Drag
$\vec{F}$: Force vector
J : Jacobian
K_δ : Hypersonic similarity parameter ($\equiv M_\infty \delta$)
L : Lift
M_∞ : Freestream Mach number
$\hat{n}$: Outward unit normal vector
N : Normal force
p : Pressure
q_∞ : Dynamic pressure
S_b : Waverider base plane area
V_∞ : Freestream velocity
$\hat{i}$, $\hat{j}$, $\hat{k}$: Cartesian base vectors
α : Angle of attack
β : Shock angle
β_s : Angle of yaw
γ : Ratio of specific heats
δ : Half cone angle
ϕ : Azimuthal angle
ϕ_s : Waverider anhedral angle
θ : Conical angle
σ : Ratio of β to δ
ξ, η, ζ : Generalized curvilinear coordinates
r, θ, ϕ : Spherical coordinates

* Department of Mechanical Engineering, College of Engineering, Mokpo National University, # 61 Dorim-ri, Chyungge-myun, Muan-gun, Cheonnam 534-729 Republic of Korea
** Aerospace and Mechanical Engineering, University of Oklahoma U.S.A.

1. Introduction

The waverider (see Fig. 1) investigated in this study is derived based on the inviscid flow over an elliptic cone. The investigation of waverider aerodynamics for the off-design performances by means of an analytical approach is almost impossible up to now. On the other hand, an experimental method would cause trouble to try to use any hypersonic wind tunnel facility because of its availability. What's more, that approach may require huge amount of expenses because the running of hypersonic wind tunnel would demand a lot of cost. Therefore, it is necessary to rely on the computational method as in this investigation.

In order to confirm the validity of the code STARS3D which is used for this study and also

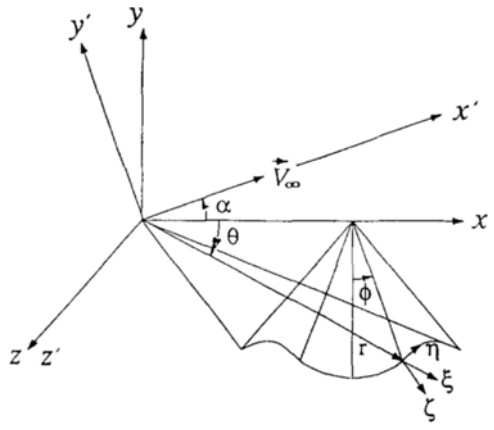

(x, y, z) = Cartesian

(r, θ, ϕ) = Spherical

(ξ, η, ζ) = Body-fitted

Fig. 1 Waverider and coordinate systems

to check the accuracy of the HSDT (Hypersonic Small Disturbance Theory) approximate method, we calculate some inviscid flow variables for circular cones and compare them with known exact solutions. As a second means of comparison, the solution of the flow past an elliptic cone is obtained by integrating the complete Euler equations numerically. Considering any waverider investigated here is constructed from the known compressible flow field past an elliptic cone at a supersonic speed, it will be profitable to obtain a flow solution about the elliptic cone in order to facilitate the understanding of waverider physics.

To check the validity of the numerical results of the flow over the waverider, it may be necessary to calculate approximate analytical solutions to the inviscid flow around an elliptic cone. The elliptic cone can be considered as a perturbed circular cone. Rasmussen et al. (Rasmussen, 1984; Kim, Rasmussen and Jischke, 1983; Rasmussen, 1994) obtained approximate solutions to the flows around circular and elliptic cones with a small angle of attack by means of perturbation theory. They were expressed by linear combination of the small perturbed terms of the eccentricity and angle of attack in the framework of the HSDT.

In studying hypersonic flows, it would be quite interesting to note that for any asymmetric supersonic or hypersonic conical flow there exists a vortical layer near the body surface where the entropy changes very rapidly. For checking the vortical layer we present entropy contours. To enhance the understanding of the waverider flows especially near the leading edges, the shock locations by both the HSDT and numerical integration for elliptic cones are calculated and presented.

The purpose of the present study is to deal with the flow fields and aerodynamics of the elliptic-cone derived waveriders by CFD (Computational Fluid Dynamics) methods utilizing the complete Euler equations. Both the fluid dynamics and aerodynamics of the waverider flow fields are of interest together with the numerics of the CFD solution method. In this study, two kinds of waverider models (Yoon, 1992) are considered. One is called Model-A which has the hypersonic similarity parameter of 0.838 (K_δ=0.838) and the other is Model-B which has K_δ=1.3. But the aerodynamic data for Model-B waverider are mainly presented.

2. Aerodynamic Forces

The normal-force and axial-force coefficients(C_N, C_A)are defined as

$$C_N=\frac{N}{q_\infty S_b},\ C_A=\frac{A}{q_\infty S_b} \tag{1}$$

where N and A are normal- and axial-forces respectively, S_b is a waverider base plane area, and q_∞ is the dynamic pressure of freestream flow. The base plane S_b is used as a reference area for comparison with experimental data which use S_b also:

$$q_\infty=\frac{1}{2}\rho_\infty V_\infty^2=\frac{1}{2}\gamma p_\infty M_\infty^2$$

$$S_b=l^2\int_{\phi=0}^{\phi=\phi_s}\tan^2\{\theta(\phi)\}d\phi \tag{2}$$

where l is the length of the waverider. The pressure force acting on a waverider can be expressed by

$$\vec{F}=\iint_S p d\vec{S}=\iint_S (p-p_\infty)\vec{n}dS \tag{3}$$

where $\hat{n}$ is an outward unit normal vector and S is a closed surface domain which embraces the whole waverider body. They are composed of three parts, i. e., a freestream upper-surface, a compression under-surface and a base plane. Now consider the definitions of normal- and axial-forces, and metrics :

$$N \equiv \hat{j} \cdot \vec{F},\ A \equiv \hat{i} \cdot \vec{F},\ d\vec{S} = \frac{1}{J} \nabla \zeta \tag{4}$$

where $\hat{i}$ and $\hat{j}$ are base vectors of body oriented coordinates. If the pressure of the base plane surface is assumed to have the freestream value, then the integration for the base plane vanishes by the second expression of $\vec{F}$ in Eq. (3). Therefore, the N and A in discretized form can now be expressed by

$$\begin{aligned} N &= 2\Sigma_{i,j}(p_\infty - p)\frac{\zeta_y}{J}\bigg|_{i,j} \\ A &= 2\Sigma_{i,j}(p_\infty - p)\frac{\zeta_x}{J}\bigg|_{i,j} \\ 1 &\le i \le i_{\max},\ 1 \le j \le j_{\max} \end{aligned} \tag{5}$$

where the subscripts i, j are for η, ζ coordinates respectively and $p_{i,j}$ denote the wall pressures on the waverider upper and lower surfaces with excluding the base plane. Note that the signs of ζ_x/J and ζ_y/J are negative for the lower compression surface where $p > p_\infty$ and thus N and A become positive. The C_N and C_A for the whole waverider body now become

$$\begin{aligned} C_N &= \frac{2}{\gamma M_\infty^2} \frac{\Sigma_{i,j}(1 - p/p_\infty)\frac{\zeta_y}{J}\Big|_{i,j}}{S_b} \\ C_A &= \frac{2}{\gamma M_\infty^2} \frac{\Sigma_{i,j}(1 - p/p_\infty)\frac{\zeta_x}{J}\Big|_{i,j}}{S_b} \end{aligned} \tag{6}$$

To get these coefficients, the summation should be carried out for the whole forebody geometry. However, for an inviscid flow over a conical body like the waveriders studied here, a simpler calculation can be done and its procedure is presented in the following procedure From the grid constructed for this problem, we can let

$$\Delta \vec{S}_j \equiv \Sigma_{i=1}^{i_{\max}} \left(\frac{\nabla \zeta}{J} \right)_{i,j} \tag{7}$$

For an inviscid flow we can apply the conical approximation such as

$$p_{i_1,j} = p_{i_2,j} \equiv p_j \tag{8}$$

where $1 \le i_1,\ i_2 \le i_{\max}$. By means of Eqs. (7) and (8), the normal-force and axial-force coefficients can be obtained as

$$\begin{aligned} C_N &= \frac{2}{\gamma M_\infty^2 S_b} \Sigma_j \left\{ 1 - \left(\frac{p_j}{p_\infty} \right) \right\} (\Delta S_y)_j \\ C_A &= \frac{2}{\gamma M_\infty^2 S_b} \Sigma_j \left\{ 1 - \left(\frac{p_j}{p_\infty} \right) \right\} (\Delta S_x)_j \end{aligned} \tag{9}$$

The ratio N/A can be easily obtained by Eq. (9) as

$$\begin{aligned} \frac{N}{A} &= \frac{\Sigma_j \{1 - p_j/p_\infty\}(\zeta_y/J)_{i_{\max},j}}{\Sigma_j \{1 - p_j/p_\infty\}(\zeta_x/J)_{i_{\max},j}} \\ &= \frac{\Sigma_j \{1 - p_j/p_\infty\}(\Delta S_y)_j}{\Sigma_j \{1 - p_j/p_\infty\}(\Delta S_x)_j} \end{aligned} \tag{10}$$

This means that it is sufficient to consider a special portion of the forebody separated by two cross sections instead of the whole forebody to calculate N/A for the forebody with conical geometry. C_L and C_D for nonzero angle of attack are calculated by the following relation :

$$\begin{bmatrix} C_L \\ C_D \end{bmatrix} = \begin{bmatrix} \cos\alpha & -\sin\alpha \\ \sin\alpha & \cos\alpha \end{bmatrix} \begin{bmatrix} C_N \\ C_A \end{bmatrix} \tag{11}$$

where C_N and C_A are based on the Cartesian coordinates (x, y, z) fixed to the waverider body.

3. Circular-and Elliptic-Cone Flow Solutions

3.1 Circular-cone flow

As test cases we calculate the shock angles β and normalized wall pressure p_w/p_∞ of inviscid circular-cone flows for several values of the basic circular-cone half angle δ. For the calculation $M_\infty = 4$ and $\gamma = 1.4$ are used. The numerical data from STARS3D code and the approximate analytic data from the HSDT (Rasmussen, 1994) are given by :

$$\frac{\beta^2}{\delta^2} \equiv \sigma^2 = \frac{\gamma + 1}{2} + \frac{1}{K_\delta^2} \tag{12}$$

$$\frac{p_w}{p_\infty} = 1 + \frac{\gamma}{2} K_\delta^2 \left(1 + \frac{\sigma^2}{\sigma^2 - 1} \ln \sigma^2 \right) \tag{13}$$

where $K_\delta \equiv M_\infty \delta$. The code STARS3D written by Scott L. Lawrence (Lawrence, 1987) was developed for integration of the parabolized Navier-Stokes equations that incorporates a steady

Table 1 Shock angle and wall pressure for $\delta=12.5°$, 17.5° and 20.0°

δ	β or p_w/p_∞	Sims	STARS3D	HSDT	ΔE_{N-E}	ΔE_{A-E}
12.5°	β	19.65°	19.72°	19.82°	+0.36%	+0.87%
	p_w/p_∞	2.307	2.306	2.349	−0.04%	+1.82%
17.5°	β	24.08°	24.16°	23.93°	+0.33%	−0.62%
	p_w/p_∞	3.368	3.365	3.451	−0.09%	+2.46%
20.0°	β	26.49°	26.42°	26.18°	−0.25%	−1.17%
	p_w/p_∞	4.006	4.002	4.130	−0.10%	+3.10%

approximate Riemann solver for the modeling of inviscid fluxes. The numerical shock position is determined by the location of the largest pressure gradient. The shock is captured with one internal grid point and it is a very clean shock without any wiggles before and after the shock. For $\delta=12.5°$, 17.5° and 20.0°, Sims tables (Sims, 1964) render exact solutions shown in Table 1.

As can be seen, the maximum percentage erroro of the approximate analytic values to the exact values (denoted by ΔE_{A-E}) for both the surface pressure and the shock angle are slightly larger than 1%. On the other hand, the maximum percentage errors of the numerical values to the exact values (denoted by ΔE_{N-E}) for the surface pressure and the shock angles are 0.1% and 0.36% respectively for the given range of δ. These indicate that the computational results are very dependable, and thus that the STARS3D code can be utilized for other similar flow calculations with confidence.

Table 2 is for two values of δ that are used to generate perturbed elliptic-cone flows. For the smaller δ case, the relative error of the analytic shock to the numerical shock (denoted by Δ_{A-N}) is positive. However, the error is negative for the larger δ case. The wall pressure data of the HSDT show consistently larger values than the exact values in Table 1 and the numerical values in Table 2.

Table 2 Shock angle and wall pressure for $\delta=12.0°$ and 18.62°

δ	β or p_w/p_∞	STARS3D	HSDT	ΔE_{A-E}
12.0°	β	19.30°	19.44°	+0.73%
	p_w/p_∞	2.217	2.257	+1.80%
18.62°	β	25.19°	24.92°	−1.07%
	p_w/p_∞	3.641	3.744	+2.83%

3.2 Entropy and vortical layer

Figures 2 and 3 show the entropy contours for the two elliptic cones generated by the basic-circular-cone half angles, $\delta=12°$ with the eccen-

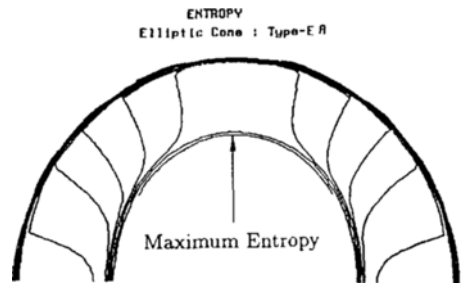

Fig. 2 Entropy contours($\delta=12°$ elliptic cone, $M_\infty=4$)

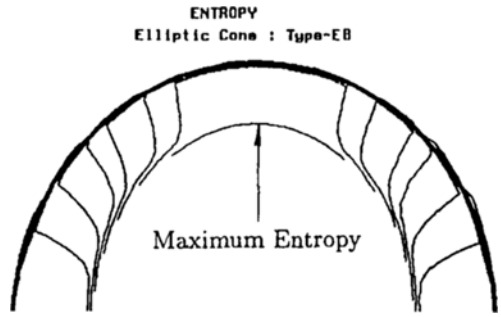

Fig. 3 Entropy contours($\delta=18.62°$ elliptic cone, $M_\infty=4$)

tricity $\varepsilon=0.1$ (Model-A) and 18.62° with $\varepsilon=0.1$ (Model-B) respectively. The constant entropy surfaces are getting closer as they approach the cone surface and they have a common tendency to embrace the body near the minor axis. (The major axis coincides with the symmetry line in those figures, and the major and minor axes meet at right angles.) This means the entropy near the wall changes very rapidly in the normal direction to the wall. A region with rapid entropy change also has a large vorticity according to Crocco's equation. The region of rapid change near the wall is called the vortical layer. According to the analysis by Ferri (Ferri, 1954), vortical singularity exists at the minor axis of an elliptic cone where multiple values of entropy occur. In order to delineate the vortical layer distinctly, of course, we need accurate entropy values on the wall and symmetry lines. In this respect a finite-difference method (FDM) would be more preferable for the purpose of capturing the vortical layer, since in a FDM both the wall and symmetry values are defined. A partially improved result for the vortical layer might be achieved by means of a finer grid in those regions.

3.3 Shock locations for elliptic cones

Figure 4 shows the shock locations for an elliptic cone (Model-A waverider generator) by the HSDT method and numerical calculation. It can be seen that the shock angle due to the approximate analytic method is greater than that obtained by the numerical integration of the Euler equations. Figure 5 shows the shock locations obtained by the above two ways or another elliptic cone (Model-B waverider generator). For this case the HSDT shock is located inside of the numerical shock. These phenomena correspond to the results of Table 2. That is, the relative shock locations by the HSDT and numerical integration for the case of both a circular cone and an elliptic cone which is generated based on the circular cone, are consistent. In those figures we can also see that the shock locations predicted by the HSDT and CFD methods are in reasonable agreement, the more so in the Model-A waverider generator.

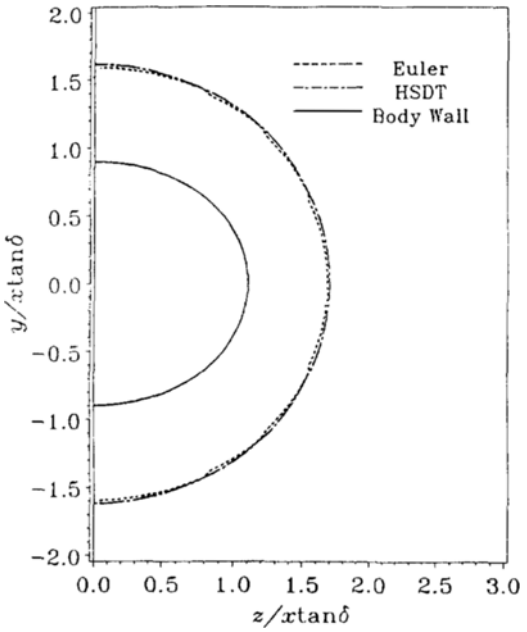

Fig. 4 Shock comparison($\delta=12°$ elliptic cone, $M_\infty=4$)

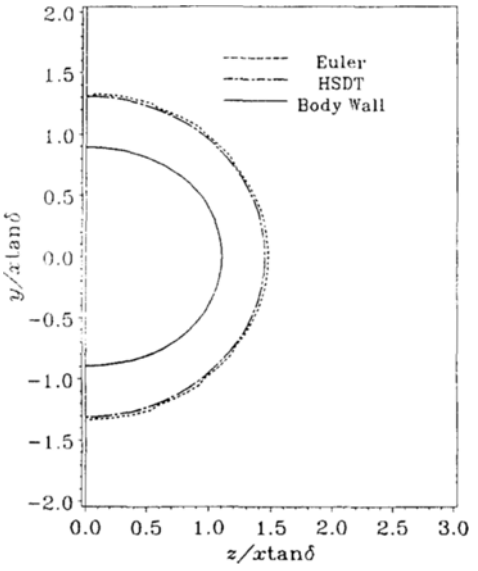

Fig. 5 Shock comparison($\delta=18.62°$ elliptic cone, $M_\infty=4$)

4. Hypersonic Flow Solution of Waverider

4.1 Entropy distribution

Figures 6 and 7 show the constant entropy

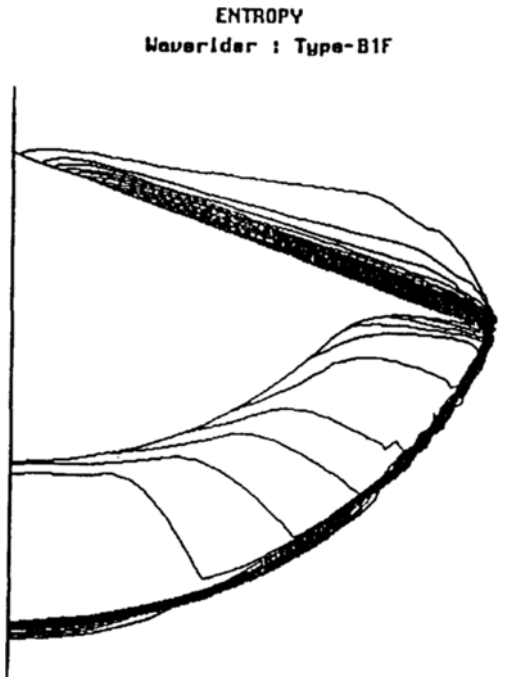

Fig. 6 Entropy contours of waverider type-BIF ($M_\infty=4$)

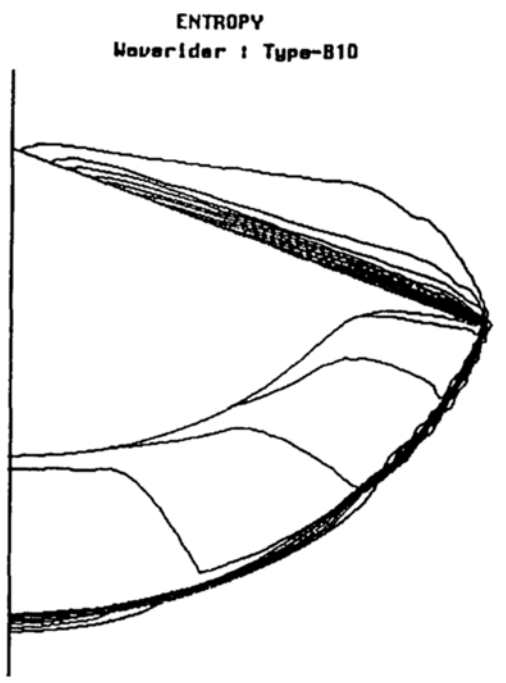

Fig. 7 Entropy contours of waverider type-BIO ($M_\infty=4$)

contours for the flows past the Model-B waverider with the two different types of grids. Figure 6 is for the Model-B waverider with a Fan-type grid (denoted by BF) and Fig. 7 for the same waverider with an O-type grid (denoted by BO). The comparison of the three plots of Figs. 3 and 6, 7 provides us one feature of entropy increase. The entropy for the waverider flow in Fig. 6 with a Fan-type grid is increased in comparison with its corresponding elliptic-cone flow in Fig. 2. This is mainly due to the sharp leading edge which makes the flow change very rapidly. Further entropy increase can be seen in Fig. 7 which is for the same waverider with an O-Type grid. The major difference between Figs. 6 and 7 is the grid structure near the tip. The O-Type grid is more skewed than the Fan-Type grid near the tip. The entropy production caused by the skewed grid may be explained in terms of a numerical viscosity. On the other hand, the entropy production by an O-Type grid is concentrated mainly on the small upper region near the tip. Because of this localized distribution of high entropy, the overall flow is not affected so much compared with the Fan-Type case except for the region of high entropy. And its effect on the shock location seems to be very little.

Again from the comparisons of entropy contours in Figs. 3 and 6, 7, it can be now seen that the constant entropy lines in Fig. 3 have similar shapes to the lower compression parts in Figs. 6, 7. This can be expected from the fact that the waverider is generated from the elliptic-cone flow. As in Fig. 3, we can observe the vortical layer near the waverider wall where the entropy gradient is large in Figs. 6, 7. A large entropy gradient can be also seen near the sharp tip. The large variation of the entropy, there would be a source of error and difficulty in the numerical calculation. Above the upper surface we can see the entropy change. This is from the shock stand-off at the leading edge. At the idealized on-design condition, the entropy of the upper region should be the freestream value. Any conical stream surface for an elliptic cone in the shock layer is composed of stream lines which originate from the same ray on the shock surface coming out of an elliptic-cone apex. We know each conical

stream surface has a constant entropy. Thus, the waverider surface should be a constant entropy surface at an idealized on-design condition. But we cannot confirm the constant entropy for the waverider surface. The partial reason for this is due to the utilization of the finite-volume method (FVM) with its pertinent boundary-condition imposition. In the FVM the flow condition is not defined at the wall and the boundary condition for the pressure is imposed by means of the linear extrapolation from the value at the center points of the first grid cells from the wall. A partially improved result would be obtained by using finer grid near the waverider surface.

4.2 Aerodynamics of waverider

The aerodynamic force coefficients at off-design Mach numbers are shown in Figs. 8, 9 and 10 at zero angle of attack for the Model-B waverider. Both the lift and drag coefficients (C_L, C_D) decrease monotonically with increasing M_∞. The lift-to-drag ratio L/D decreases from 3.52 to 3.27, as M_∞ increases from 3 to 5. For this Mach number range, the variation of aerodynamic forces with respect to freestream Mach number is significant.

Also shown in those figures are the on-design results ($M_\infty=4$, $\alpha=0°$) by the experiment (Rasmussen, Jischke, Daniel, 1982), the full-potential equation (Jones, 1986) and the HSDT approximation for the idealized cone-derived waverider. At the on-design condition, C_L from the Euler equations is about 3.6% lower than the result for the full-potential equations, and about 9.6% lower than the experimental result. The on-design value of C_D from the Euler equations is about 13.7% lower than the result for the full potential equations, and about 19.5% lower than the experimental result. It should be noted that the experimental result includes a contribution from viscous effects. The L/D ratio according to the Euler calculations are 13.4% greater than for the full-potential equations and 7.3% greater than the experimental result.

Now it should be mentioned that the standard of comparison for checking the accuracy of the Euler solution obtained in this study is not the

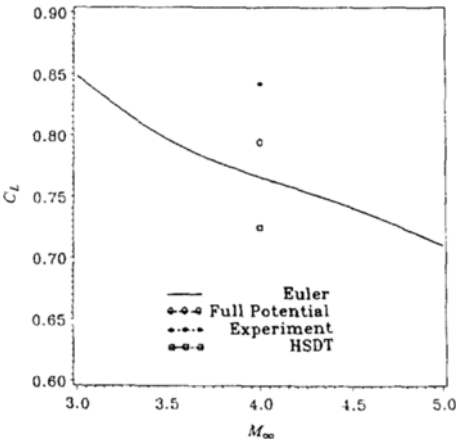

Fig. 8 Lift coefficient vs. $M_\infty(\alpha=0°)$

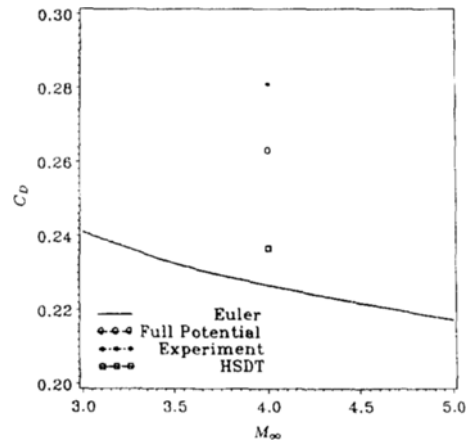

Fig. 9 Drag coefficient vs. $M_\infty(\alpha=0°)$

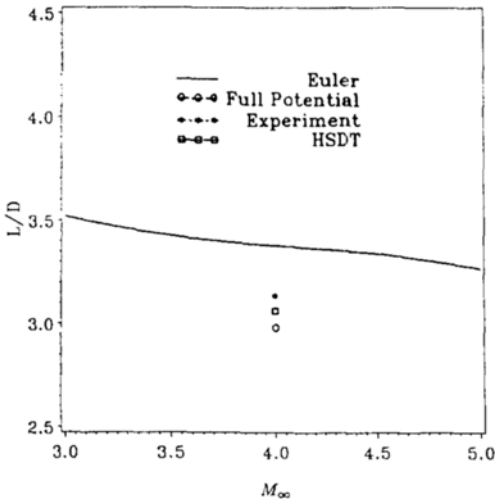

Fig. 10 Lift/drag ratio vs. $M_\infty(\alpha=0°)$

experiment but the HSDT solution. There are a couple of reasons for that. Firstly, the waverider configuration studied here is constructed inversely from the HSDT solution of hypersonic flow around an elliptic cone. Secondly, both HSDT and Euler solutions are for inviscid flows, but the experimental data are related to real viscous flows. The above assertion now can be assured by Figs. 8, 9. If we make comparison on the basis of experimental data in those figures, it appears that the full potential results are better than the Euler results. But this is not true at all, since the standard of comparison should be simply HSDT rather than the experiment, as explained above. However, if we compare on the basis of the HSDT, we can easily recognize that the Euler solver shows better agreement with the HSDT than the full potential solver does. That's just what we expect in this study.

The normal-force coefficient in the y-direction C_N and the axial-force coefficient in the x-direction C_A as a function of α for $M_\infty=4$, are shown in Figs. 11, 12. The comparison of C_N in Fig. 11 of numerical and experimental data (Rasmussen, Jischke, Daniel, 1982) shows very good agreement, and C_N varies almost linearly. Figure 12 illustrates C_A vs. α. As expected, the numerical data are lower than the experimental data, since the C_A of viscous flow has an additional contribution due to the skin friction.

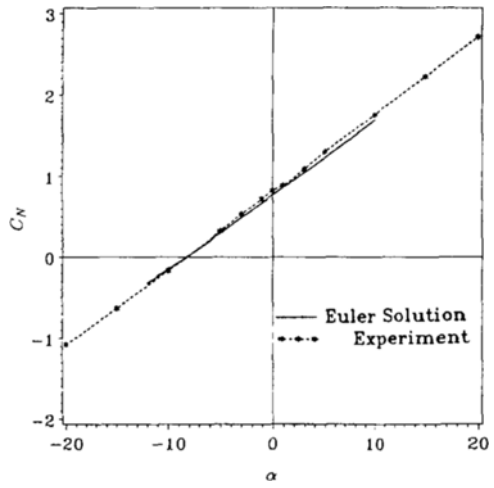

Fig. 11 Normal-force coefficient vs. $\alpha(M_\infty=4)$

Figures 13, 14 and 15 show aerodynamic quantities C_L, C_D and L/D for the elliptic-cone waverider Model-B as functions of angle of attack α at the designed Mach number of 4. It is known (Rasmussen) that the lift/drag ratio of viscous flow for an idealized cone waverider, for example, which has infinitesimally thin winglets, approaches the value of its corresponding inviscid flow as the cone deflection angle δ increases. The waverider investigated here has $\delta=18.62°$ for which the difference of lift/drag ratio between inviscid and viscous flows is small, that is, the viscous drag is much smaller than the wave drag. This indicates that the comparison of the numeri-

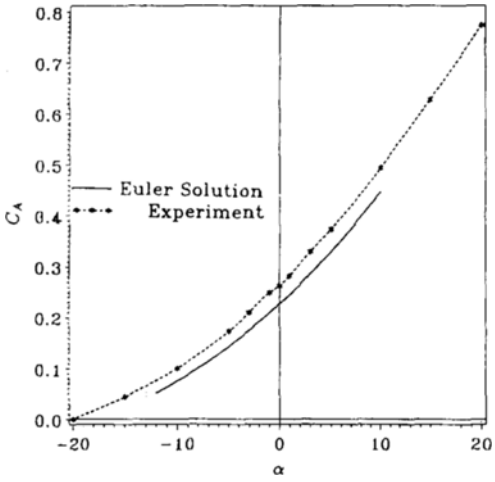

Fig. 12 Axial-force coefficient vs. $\alpha(M_\infty=4)$

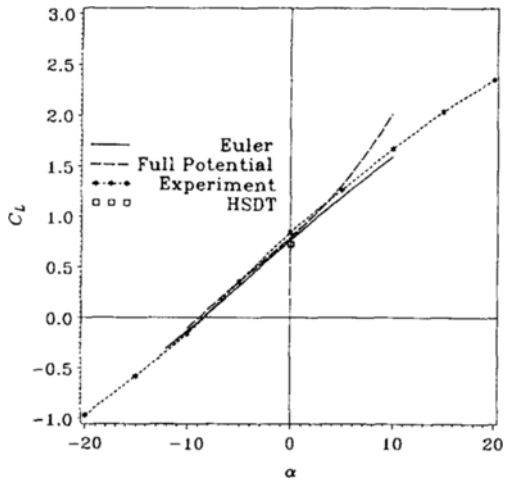

Fig. 13 Lift coefficient vs. $\alpha(M_\infty=4)$

cal inviscid solutions with the experimental viscous results can be justified accordingly.

Figure 13 shows the lift coefficients C_L as a function of angle of attack at the on-design Mach number 4. The agreement of the numerical results obtained by solving the complete Euler equations with experimental data is quite good for the range of α from $-12°$ and $10°$. Approximately, C_L increases linearly with α. As α decreases, C_L also decreases and becomes zero at $\alpha \cong -8.5°$. For negative α, the full-potential result is very close to the experimental data, but the accuracy declines as α increases in the positive region. These phenomena can be expected from the theoretical restrictions on the potential theory. As α becomes a larger positive value, the effective flow deflection angle becomes much larger. This causes the flow to be more nonlinear and to increase the rotationality. Accordingly, the homentropic approximation which is assumed in the full potential theory becomes worse, as α increases. On the other hand, negative angles of attack do not increase the effective flow deflection angle for the range of α used here, considering that at the on-design condition the centerline of the waverider($\cong \delta/2$) has already positive deflection to the freestream direction and the negative angle of attack is compensated by this deflection more or less. This is the reason why the agreement is good for negative angles of attack.

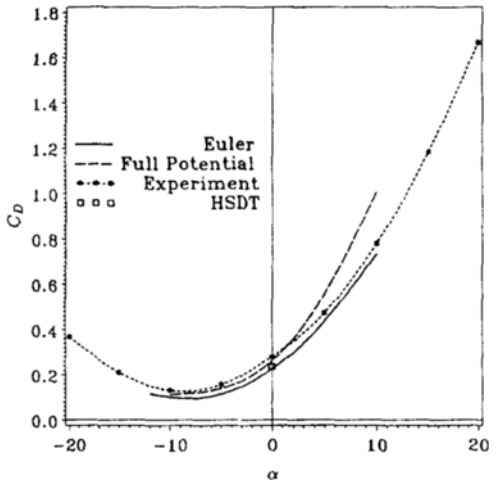

Fig. 14 Drag coefficient vs. $\alpha(M_\infty=4)$

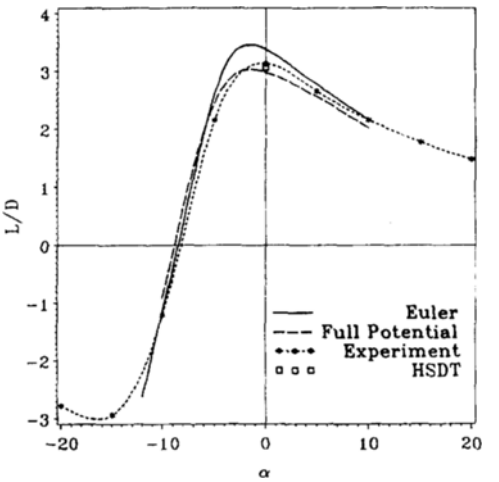

Fig. 15 Lift/drag ration vs. $\alpha(M_\infty=4)$

In short, as the hypersonic similarity parameter K_δ (proportioned directly to effective deflection angle δ) becomes larger, the full potential method gives much worse results. Suppose any flow has a larger value of K_δ, then this flow shows more hypersonic charateristic. From this point of view, the full potential method may seem to be reasonably good for supersonic flows, but bad for hyperonic flows.

The drag coefficients C_D are plotted in Fig. 14 with the same conditions as in Fig. 13. The variation resembles a parabolic shape about α of zero lift value. The numerical values are lower than the experimental data, as expected. For the positive angles of attack, there is considerable discrepancy between the full-potential result and the experimental data, again as for C_L.

The L/D ratios are depicted in Fig. 15. The maximum value of L/D for both the Euler and full-potential calculations occurs at $\alpha \cong -2°$, whereas the maximum value for the experimental results occurs at $\alpha \cong 0°$ (the on-design condition). In principle, the L/D for inviscid flow should be greater than that for viscous flow, since viscosity increases the drag while affecting the lift only a small amount. The Euler results are in accord with this whereas the full-potential results are not, at least for $\alpha > -2°$. Systematic errors in the calculation of C_L and C_D tend to compensate when the ratio is taken to obtain L/D. This is especially true for the calculation of the reference

area since it cancels out entirely for the L/D ratio.

So far only the Model-B waverider has been discussed. To anticipate the L/D ratio for another type waverider, it would be useful to consider an idealized cone waverider which has infinitesimally thin winglets. The L/D for such a waverider can be obtained from reference (Kim, Rasmussen, Jischke, 1983) as

$$L/D=\frac{\sin\phi_s}{\delta\phi_s}\frac{4\sigma^2/(\sigma+1)}{1+\sigma^2\ln\sigma^2/(\sigma^2-1)} \qquad (14)$$

The Model-A waverider has smaller δ and ϕ_s than Model-B. According to Eq. (12), these smaller values provide larger L/D ratio for Model-A. Actually the on-design numerical value of L/D for Model-A is 6.52, which is much greater than 3.38 for Model-B waverider. Those values of L/D due to Eq. (12) are slightly less than the above numerical results for elliptic-cone waveriders.

5. Concluding Remarks

Through the numerical integration of the full Euler equations, some important results were obtained. Firstly, the entropy distributions around waveriders provided vortical layers and helped to analyze the exact shock location as well. At this point, it should be noted that the vortical layer of waveriders has not been known up to now. Secondly, the various aerodynamic forces for a wide range of variations in angles of attack and freestream Mach numbers were obtained in this study. The comparison of lifts and drags with existing experimental data, the numerical results of this study showed excellent agreement in their trends and quite good agreement in data themselves. These aerodynamic data could be useful for the design of high speed airplanes such as National Aero-Space Plane(NASP) which is being under investigation in the United States of America. Thirdly, it was clarified that the lift to drag ratio calculated by the hypersonic small disturbance theory which was presented in this paper implied hidden errors, but they seemed to be very minor and turned out to be correct. The reason is that the errors by the lift and the drag, although each of which contains a quite big discrepancy, were cancelled by plus and minus error effects.

Acknowledgments

This work was supported by NASA Langley Grant No. NAG-1-886. The authors appreciate the support.

References

Doty, R. T. and Rasmussen, M. L., 1973, "Approximation for Hypersonic Flow Past an Inclined Cone," *AIAA J.*, Vol. 11, No. 9, pp. 1310~1315.

Jones, K. M., 1986, "Application of a Full Potential Method for Predicting Supersonic Flowfields and Aerodynamic Characteristics," *J. of Spacecraft and Rockets*, Vol. 23, No. 1, Jan.-Feb., pp. 63~69.

Kim, B. S., Rasmussen, M. L. and Jischke, M. C., 1983, "Optimization of Waverider Configurations Generated from Axisymmetric Conical Flows," *J. of Spacecraft and Rockets*, Vol. 20, No. 5, pp. 461~469.

Lawrence, Scott L., 1987, "Application of an Upwind Algorithm to the Parabolized Navier-Stokes Equations," Ph. D. Dissertation, Iowa State University.

Rasmussen, M. L., 1994, Hypersonic Flow, Wiley-Interscience, New York.

Rasmussen, M. L. and Lee, H. M., 1979, "Approximation for Hypersonic Flow Past a Slender Elliptic Cone," *AIAA Paper* 79-0364, *17th Aerospace Sciences Meeting.*

Rasmussen, M. L., Jischke, M. C. and Daniel, D. C., 1982, "Experimental Forces and Moments on Cone-Derived Waveriders for $M_\infty=3$ to 5," *J. of Spacecraft and Rockets*, Vol. 19, No. 6.

Sims, J. L., 1964, "Tables for Supersonic Flow around Right Circular Cones at Zero Angle of Attack", *NAS 1.21 NASA SP*-3004.

Yoon, B-H., 1992, "On-design Solutions of Hypersonic Flows past Elliptic-Cone Derived Waveriders," *KSME Journal*, Vol. 6, No. 1, pp. 24~30.